European Journal of Pharmaceutics and Biopharmaceutics 109 (2016) 81–92

Contents lists available at ScienceDirect

European Journal of Pharmaceutics and Biopharmaceutics

journal homepage: www.elsevier.com/locate/ejpb

Inhibition of carbonic anhydrase IX in glioblastoma multiforme

Abdolali Amiri [a], Phuong Uyen Le [b], Alexandre Moquin [a], Gayane Machkalyan [a], Kevin Petrecca [b,*], John W. Gillard [a,c], Nathan Yoganathan [c], Dusica Maysinger [a,*]

[a] Department of Pharmacology and Therapeutics, McGill University, Montreal, Quebec H3G 1Y6, Canada
[b] Department of Neurology and Neurosurgery, Montreal Neurological Institute and Hospital, McGill University, Montreal H3A 2B4, Quebec, Canada
[c] Kalgene Pharmaceuticals, Innovation Park at Queens University, Kingston K7L 3N6, Ontario, Canada

ARTICLE INFO

Article history:
Received 18 April 2016
Revised 6 September 2016
Accepted in revised form 28 September 2016
Available online 1 October 2016

Keywords:
Glioblastoma spheroid
Brain tumor stem cells
Carbonic anhydrase IX
Drug delivery system
Acetazolamide
Temozolomide

ABSTRACT

Carbonic anhydrase IX (CA IX) is a transmembrane enzyme upregulated in several types of tumors including glioblastoma multiforme (GBM). GBM is among the most aggressive tumors among gliomas. Temozolomide (TMZ) therapy combined with surgical or radiation approaches is the standard treatment but not effective in long term. In this study we tested the treatment with acetazolamide (ATZ), an inhibitor of CA IX, alone or combined with TMZ. The experiments were performed in 2D and 3D cultures (spheroids) using glioblastoma U251N and human brain tumor stem cells (BTSCs). Several proteins implicated in tumor cell death were also investigated. The key results from these studies suggest the following: (1) Cell death of human glioblastoma spheroids and BTSC is significantly increased with combined treatment after 7 days, and (2) the effectiveness of ATZ is significantly enhanced against BTSC and U251N when incorporated into nano-carriers. Collectively, these results point toward the usefulness of nano-delivery of CA IX inhibitors and their combination with chemotherapeutics for glioblastoma treatment.

1. Introduction

Carbonic anhydrase IX (CA IX) is a transmembrane enzyme upregulated in several types of tumors including glioblastoma multiforme (GBM). Glioblastoma multiforme (GBM) is a primary brain tumor which is one of the most common and aggressive brain tumors [1]. The survival rate with the standard of care, maximal surgical resection and radiotherapy in conjunction with chemotherapy is about 6–12 months [2]. A common feature of the solid tumors, including glioblastomas, is their hypoxic environment which results from structurally abnormal and functionally unstable tumor vasculature, leading to a poor oxygen delivery to the growing tumors of high oxygen demand [3,4]. To grow and to survive in this hostile environment, a highly conserved hypoxia-induced intracellular signaling cascade, regulated by transcription factor hypoxia inducible factor 1 and 2 (HIF1/2), is activated by the stressful hypoxic cells in the tumors [4]. Activation of HIF pathway modulates a number of proteins critically involved in tumor progression [5–7], including CA IX [8–10].

CA IX is an integral transmembrane enzyme which is composed of 4 domains: the N-terminal proteoglycan domain controlling cell attachment [11], the extracellular catalytic domain, a hydrophobic trans-membrane region, and a cytoplasmic tail [12]. CA IX catalyzes the reversible conversion of carbon dioxide to carbonic acid ($CO_2 + H_2O$ to HCO_3^- and H^+). Among all 15 human α-carbonic anhydrases, CA IX has the highest catalytic activity and the exposure of its catalytic domain to the extracellular domain allows an indirect contribution to the intra-extracellular pH by production of bicarbonate, regulated by bicarbonate/chloride exchange [13,14]. CA IX plays critical roles in tumor cells, including cell survival and proliferation, stem cell phenotype maintenance [15], epithelial-mesenchymal transition (EMT) in carcinoma cells [16], invasion, metastasis [17], and resistance to radiation therapy and chemotherapy [18–21]. Importantly, the accumulation of acidic by-products such as lactic acid, produced by highly metabolic cancer cells involved in glycolytic metabolism, leads to the presence of an increasingly acidified intracellular pH and basic extracellular pH [6,22,23].

Several studies have established that depletion of CA IX gene expression and inhibition of its catalytic activity in the context of hypoxia dysregulate pH homeostasis and affect the viability of several types of cancer cells *in vitro* [21,24]. Studies in several human tumor cell lines with constitutive or upregulated CA IX expression

* Corresponding authors at: Department of Pharmacology and Therapeutics, McGill University, Montreal, Quebec H3G 1Y6, Canada.
E-mail address: dusica.maysinger@mcgill.ca (D. Maysinger).

http://dx.doi.org/10.1016/j.ejpb.2016.09.018
0939-6411/

in hypoxia, show that selective CA IX inhibitors cause a decrease in intracellular pH (acidification), and enhancement of the extracellular pH (alkalinization) [18,25–28].

The objective of this study was to employ glioblastoma cells in 2D and 3D and in spontaneously formed clusters of brain tumor stem cells, to evaluate effectiveness of CA IX inhibitors, individually and in combination with the first-line therapeutic anticancer agent, temozolomide (TMZ) [29]. A combination therapy was particularly effective against brain tumor stem cells, when acetazolamide (ATZ), a CA IX inhibitor was incorporated into a polymeric poly(ethylene glycol)-*block*-poly(lactide-*co*-glycolide) (PEG-PLGA) nano-carrier, in 3D spheroid models.

2. Materials and methods

Solutions, media and reagents. 3-(4,5-dimethylthiazol-2-yl)-2,5-diphenyl tetrazolium bromide (MTT), Hoechst 33342, Rhodamine B-isothiocyanate, PEG-PLGA, propidium iodide (PI), acetazolamide (A6011-10G), temozolomide (T2577), and goat serum (G-9023) were purchased from Sigma-Aldrich (Oakville, ON, Canada). U251N human glioblastoma cell line was provided by Dr. Josephine Nalbantoglu (Montreal Neurological Institute, Montreal, QC, Canada). U251N cell line was originally obtained from the American Type Culture Collection. Human IgG1 anti-CA IX (1.8 mg/mL, Ab ~ 150 kDa) was acquired from Dr. Nathan Yoganathan (Kalgene Pharmaceuticals, Kingston, Ontario). Mouse anti-human CA IX-MAb was purchased from Abcam® (Cambridge, MA, USA Cat# ab107257). Cell culture media, penicillin-streptomycin, and heat-inactivated fetal bovine serum (FBS) were purchased from Invitrogen (Burlington, ON, Canada).

2.1. Cell cultures

Brain tumor stem cell (BTSC) 3D-clusters. Human glioblastoma stem cells (hGSC) were isolated as previously performed by Kelly et al. and expanded in neurosphere cultures [30]. 48EF and 84EF were kindly provided by Dr. Samuel Weiss (University of Calgary, AB, Canada). hGSC spheres were cultured in complete Neurocult™-NS-A proliferation medium (Neurocult™ basal medium containing: Neurocult™ NS-A proliferation supplement, 20 ng/mL rh EGF, 20 ng/mL rh bFGF, and 2 μg/mL Heparin) from StemCell™ Technologies Inc. (Vancouver, BC, Canada). When spheres appeared large enough for passaging (<300 μm in diameter), they were collected in tubes and spun at 1200 rpm for 3 min. To dissociate the spheres, 800 μL of Accumax® (Millipore®, Burlington, MA, USA) was added to the cell pellet and incubated for 5 min at 37 °C, washed with PBS, centrifuged and re-suspended in complete Neurocult™-NS-A proliferation medium and seeded at a concentration of 200,000 cells/flask.

U251N human glioblastoma monolayers were cultured in Dulbecco's Modified Eagle Medium (DMEM; Gibco®, Life Technologies Inc., Burlington, ON, Canada) supplemented with 10% (v/v) FBS (Gibco®) and 1% (v/v) penicillin–streptomycin (Gibco®). Cells were seeded 24 h before treatment according to the appropriate density for the indicated assay (described in detail below). They were maintained at 37 °C with 5% CO_2 and 95% relative humidity.

Spheroid formation. Spheroid cultures were prepared using a protocol adapted from the liquid overlay system previously established by Dhanikula et al. [31]. Confluent U251N monolayer cell cultures were detached using 0.05% trypsin-EDTA (Gibco), and seeded at 5000–50,000 cells per well in 96-well plates precoated with 2% agarose (Invitrogen) in serum-deprived DMEM solution. Spheroids were seeded and maintained in filtered (0.22 μm) complete DMEM medium for four days before drug treatment with ATZ (alone or encapsulated in micelles), TMZ and the MAb-CA IX. 100 μL of filtered, complete DMEM medium was replaced every four days.

Cell treatment. Confluent monolayer cell cultures were detached using 0.05% trypsin-EDTA, and seeded in 24-well-plate (Costar®, Corning Inc., Corning, NY, USA) at 20,000, 10,000 or 5000 cells per well (for 1, 3, and 6 days treatments, respectively) or seeded in 6-well plates (Corning Inc.) at 100,000 or 300,000 cells per well (for 1 and 6 day-treatments, respectively), and treated after 24 h.

For chemical induction of hypoxia, cells were treated with 50 μM cobalt chloride ($CoCl_2$) dissolved in sterile pure water, for 24 h before addition of TMZ (100 μM), ATZ (100 μM), MAb-CA IX (Kalgene, 5 nM), or their combinations (for 1–6 days). Spheroids have hypoxic cores; therefore, the same drug concentrations were used in the absence of $CoCl_2$.

Stock solutions of temozolomide (Sigma-Aldrich; 43 mM) and acetazolamide (Sigma-Aldrich; 200 mM) were prepared in dimethyl sulfoxide (DMSO; Sigma-Aldrich), and were added to cells for a final DMSO concentration of <0.5%. $CoCl_2$ was dissolved in pure water. MAb-CA IX (Kalgene; 12 μM) stock was dissolved in PBS.

MTT assay. Following treatment, the culture medium was replaced with serum-deprived DMEM containing thiazolyl blue tetrazolium (MTT, 0.5 mg/mL; Sigma-Aldrich). The cells were incubated at 37 °C for 60 min to allow for formazan formation, after which the medium was removed, and dimethyl sulfoxide (DMSO; 500 μL; Sigma-Aldrich) was added to dissolve the formazan crystals. Samples were collected in triplicate, and the absorbance was measured at 595 nm using a microplate reader (Benchmark™; Bio-Rad, Mississauga, ON, Canada).

XTT assay. BTSCs were plated at 10,000 cells/well in 96 well overnight in culture media. Drugs (ATZ, TMZ, and ATZ-micelles) were added to their final concentrations in a final volume of 200 μL. After indicated time of incubation at 37 °C, 50 μL of XTT was prepared as instructed by the manufacturer (Life Technologies Inc.) and the mixed XTT solution was added and further incubated for 2 h at 37 °C. The absorbance at 490 nm was measured on an Epoch™ plate reader (BioTek, Winooski, VT, USA).

Hoechst 33342 and propidium iodide labeling. In monolayer cultures, Hoechst 33342 (10 μM) and propidium iodide (PI, 1.5 μM) were added to the culture medium following the treatments and incubated at 37 °C for 60 min. Analysis of the plates was immediately followed. Cell imaging was conducted using an automated microscopy platform (Operetta™ High Content Imaging System; Perkin Elmer, Waltham, MA, USA). Image analysis and cell counting were performed using the Columbus Image Data Storage and Analysis platform (Perkin Elmer).

Hoechst 33342 (10 μM) and PI (1.5 μM) fluorescent dyes were added 4 h prior to measurements in spheroid cultures. Following treatment, individual spheroids were carefully transferred onto a microscope slide using a pipette and flattened under a coverslip; cell number was assessed. A total cell number corresponded to all Hoechst-labeled nuclei and only cells with damaged plasma membranes were labeled with PI. Imaging was conducted using a fluorescence microscope (Leica, Wetzlar, Germany). Fluorescence intensity and cell numbers were quantified using ImageJ software [32], and CyQuant® software (Thermo Fisher Scientific, Waltham, MA, USA).

Caspase-3 activity measurement. EnzCheck caspase-3 assay kit #2 (E13184, Molecular Probes, Eugene, OR, USA) with some minor changes to its protocol was used to measure caspase-3 activity as described below. Following the treatments, the culture medium was collected. Cells were washed twice with PBS and detached using 0.05% trypsin-EDTA. The cells were collected and added to their respective culture medium. They were centrifuged at 12,000 rpm for 4 min. 50 μL of the 1× lysis buffer (1.5 mL of 200 mM TRIS, pH 7.5, 2 M NaCl, 20 mM EDTA, 0.2% TRITON™ X-100) was added to each pellet and re-suspended. The suspension

of cells was frozen at −80 °C and thawed subsequently. The cells were centrifuged at 12,000 rpm for 4 min. 50 μL of the supernatant from each treatment was then transferred to a 96 well plate (Sarstedt, Nümbrecht, Germany). 50 μL of the reaction buffer (50 mM PIPES, pH 7.4, 10 mM EDTA, 0.5% CHAPS) at 5× diluted down to 2× by ddH_2O containing 20 mM DTT was added to each supernatant followed by 30 min incubation at room temperature. The controls contained 50 μL of the lysis buffer and 50 μL of the reaction buffer (2×) with 10 mM DTT. Spectrofluorometric measurements (in triplicate) were done with excitation/emission wavelengths set at ~496/520 nm (FLUOstar OPTIMA, BMG LABTECH GmbH, Ortenberg, Germany).

Western blotting. U251N glioblastoma cells were seeded at a density of 300,000 per well into six-well cell culture plates and left to adhere for 24 h in a final volume of 2 mL serum-supplemented DMEM media (10% FBS, 1% Pen-Strep). The drugs and the nanocarriers were added to the adherent monolayers in the concentrations ranging from 10 to 100 μM for 1–6 days as indicated in individual figure legends. Following treatment, cells were trypsinized, pelleted, resuspended in lysis buffer (10 mM sodium phosphate pH 7.0, 150 mM NaCl, 1% NP40, 0.1% SDS, 1% sodium deoxycholate, 10 mM NaF, 2 mM EDTA), centrifuged and followed by the collection of the supernatant. For spheroids, following the treatments, they were picked up by a pipette, pelleted and resuspended in the lysis buffer. 10–20 μg of protein (measured by Bradford® protein assay (Bio-Rad)) was loaded onto a 12% sodium dodecyl sulfate-polyacrylamide gel and transferred to a PVDF membrane. Membranes were washed with 0.1% Tween®-20 + TBS and blocked with 3% milk (with 1:10,000 of 10% NaN_3) + 0.5% Tween®-20 + TBS for 1 h at room temperature. Membranes were then incubated with primary antibodies (anti-CA IX McAb dilution 1:1000) in blocking solution overnight at 4 °C. After three washes with 0.1% Tween®-20 + TBS, the membranes were incubated with the HRP-conjugated anti-rabbit/mouse (Bio-Rad) diluted 1:5000 in 3% milk (with 1:10,000 of 10% NaN_3) + 0.5% Tween®-20 + TBS for 1 h at RT. After three washes with 0.1% Tween®-20 + TBS, HRP substrate (Luminata™, Millipore) was added and incubated for 5 min, following which the membranes were exposed to HyBlot CL® film (Harvard Bioscience, Holliston, MA, USA). Blotting with mouse anti-actin (dilution 1:5000, Millipore) was used as a housekeeping protein to control for consistent protein loading. Densitometry was performed using ImageJ [32] and data were tabulated and graphed using the Microsoft Excel®.

Acetazolamide incorporation into polymeric nanoparticles. ATZ-loaded micelles were prepared by dissolving poly(ethylene glycol) methyl ether-*block*-poly(lactide-*co*-glycolide) (PEG M_n 2000 Da, PLGA M_n 4000 Da) and acetazolamide in acetone with sonication (3 min) to obtain a clear solution (5 mg/mL of ATZ and 10 mg PEG-PLGA). An equal volume of water was placed in a vial with a magnetic stirrer. The acetone solution containing polymer alone or a mixture of polymer with drug was added dropwise (10 μL/s) into the water under constant agitation. The vial was left uncapped with constant agitation for 24 h and then placed under vacuum overnight to remove any traces of acetone. Non-encapsulated acetazolamide formed precipitates which were removed by centrifugation at 2000*g* for 5 min. The mass of non-encapsulated acetazolamide (precipitate) was weighed after freeze-drying the pellet in a VirTis Sentry Benchtop™ 3L vacuum pump (SP Industries, Gardiner, NY, USA). The sizes of the blank and acetazolamide-loaded micelles were determined by asymmetrical flow field-flow fractionation (AF_4, Dualtec®, Wyatt Technology, Santa Barbara, CA, USA) coupled to a UV–vis detector and a dynamic light scattering detector (Wyatt, QELS).

AF_4 protocol. The AF_4 separation was performed on an Agilent® 1100 (Agilent Technologies, Waldbronn, Germany) combined with a short channel (SC) separation channel linked to Wyatt Eclipse DualTec™ (Wyatt Technology, Santa Barbara, CA, USA), coupled with a UV–vis detector SPD-20A (Shimadzu Co., Kyoto, Japan), a fluorescence detector (RF-10AXL, Shimadzu Co.), and a quasi-elastic light scattering (QELS) detector (WyattQELS™, Wyatt Technology) which is an add-on unit connected to the MALS Dawn Heleos™ 8+ detector (Wyatt Technology). The MALS was equipped with a K5 cell and a GaAs laser operating at 658 nm. The separation channel was equipped with a 350 μm spacer (Wyatt Technology), a length of 15.5 cm and a width from 2.1 to 0.1 cm and a regenerated cellulose membrane with a cut-off of 10 kDa from Microdyn-Nadir (Wiesbaden, Germany). The samples were measured at 0.5 s intervals and the UV and MALS signals were simultaneously recorded as fractograms, plots of detector signal intensity versus time. Data acquisition and processing were performed using ASTRA® ver. 6.1.1.17 (Wyatt Technology).

The retention times of PEG-PLGA micelles and the drug were evaluated in phosphate buffer (10 mM, pH 7.4). The buffer was filtered (0.1 μm Whatman® filter, GE Healthcare Life Sciences, Pittsburgh, PA, USA) prior to use.

The flow rate at the detector was kept constant at 0.5 mL/min throughout the run. The elution profile was the following: (1) Elution step with a crossflow set at 1.5 mL/min for 1 min; (2) Focus step for 2 min with a crossflow set at 1.5 mL/min; (3) Focus + Inject step for 2 min with a crossflow set at 1.5 mL/min; (4) Focus step for 1 min with a crossflow set at 1.5 mL/min; (5) Elution step for 15 min with a crossflow decreasing linearly from 1.5 mL/min to 0 mL/min; and (6) Elution step for 15 min with a constant crossflow set at 0 mL/min. The last elution step was used to flush out any large particles.

The detection of the eluted fractionated polymers and drug was performed sequentially by UV absorbance at 265 nm, MALS (measure radius of gyration, R_g), and DLS (measure the radius of hydration, R_H). The Z-average effective spherical hydrodynamic radius of the eluting particles/agglomerates was determined by DLS based on cumulant analysis of the scattered intensity correlation functions measured across each eluting band. Each fractogram presented is representative of a triplicate sample.

Fluorescent labeling of polymeric nanoparticles. PEG-PLGA diblock was labeled with rhodamine-B isothiocyanate by direct reaction with the —OH terminal group of PLGA. PEG-PLGA (0.01 mmol) was dissolved in dichloromethane (1 mL). Rhodamine B-isothiocyanate (0.5 μmol) was dissolved in dichloromethane and then added to the PEG-PLGA solution. The reaction proceeded for 10 h at room temperature. The excess rhodamine B was removed by dialysis first in ethanol, followed by a second dialysis in distilled water (M_w cut off: 5 kDa). The labeled polymer solution was then lyophilized (SP Industries). Micelles were prepared following the same procedure as described above.

Uptake of Rhodamine-labeled micelles. U251N spheroids were generated by plating 5000 cells/well on a 96 well plate pre-coated with 2% agarose (Invitrogen) using *in vitro* liquid overlay system as described above [31]. To evaluate micelle uptake, spheroids were incubated with both unloaded and ATZ-loaded Rhodamine-B-labeled micelles and ATZ alone. Spheroid treatments started 4 days post-seeding. All treatments were done with drugs in freshly supplemented medium (DMEM + 1% FBS). Micelle-incorporated ATZ (1 μM ATZ in 0.6 μg/mL micelles, 10 μM ATZ in 6 μg/mL micelles, and 100 μM ATZ in 60 μg/mL micelles) was incubated in 96 well plates at 5% CO_2, 37 °C for 24 h, 3 days, and 6 days. Following treatment, individual spheroids were carefully transferred onto a microscope slide using a pipette, and flattened under a coverslip. Imaging was conducted using a fluorescence microscope (Leica), and corrected total fluorescence (CTF) intensity was quantified using ImageJ [32] software following CTF = Inte-

grated Density – (Area of selected cell × Mean fluorescence of background readings).

Statistical analysis. Data were graphed and tabulated using Microsoft Excel®. Each experiment was repeated at least twice and each drug treatment was performed in triplicate (in 24-well plates), or in five or six samples (in 96-well plates). All data are expressed as mean ± S.E.M. The Student's *t*-test with Bonferroni correction was used to analyze significant differences between two group means (p values < 0.05 were considered to be significant) using GraphPad Prism®.

3. Results

3.1. Effect of combination of ATZ and TMZ treatment on U251N monolayers

CA IX was proposed as a biomarker of hypoxia in several tumor types [33]. In order to establish the hypoxic conditions in monolayer glioblastoma cells U251N, $CoCl_2$ (10–100 μM) was used in different concentration as an inducer of chemical hypoxia (Fig. S1A). $CoCl_2$, enhanced CA IX in a dose dependent manner, starting at 10 μM $CoCl_2$ after 3-day treatment as determined by Western blot (Fig. S1B). CA IX expression induced by $CoCl_2$ was suppressed when cells were treated concomitantly with ATZ (Fig. S1B).

Having established the appropriate hypoxic conditions for CA IX induction in monolayers, we then investigated the relationship between the CA IX expression and cell viability in U251N cultures in the presence and absence of CA IX inhibitor ATZ.

U251N cell viability (in the monolayers) did not significantly change upon exposure to the drug treatments under normoxia or hypoxia within the initial 24 h treatment with ATZ (100 μM), TMZ (100 μM), or their combination (Fig. 1B). However, after three days of exposure to TMZ alone, or in combination with ATZ (100 μM), or the anti-CA IX antibody (5 nM), there was a reduced cell viability (47 ± 5% ($p < 0.05$), 44 ± 6% ($p < 0.05$), and 39.8 ± 0.4% ($p < 0.01$), respectively) under hypoxic conditions (Fig. 1B). Although ATZ treatment alone for 6 days did not significantly decrease cell viability under either normoxic or hypoxic conditions, it caused a significant cell death when combined with TMZ (100 μM), under both of these conditions (Fig. 1B). The reduction in cell viability was moderately, but significantly higher, for ATZ (100 μM) and TMZ (100 μM) combined when compared to the TMZ (under normoxic (19 ± 2% ($p < 0.05$), and 25 ± 2% ($p < 0.05$), respectively) and hypoxic conditions (13.9 ± 0.6% ($p < 0.01$), and 20 ± 2% ($p < 0.01$), respectively). Photomicrographs (Fig. 1A) indicate some picnotic and hypertrophic nuclei labeled with PI, suggesting several modes of cells death caused by the treatments. Reduction of mitochondrial metabolic activity in U251N cells treated with the aforementioned drugs was correlated with reduction of cell number as determined by cell counting of fluorescent nuclei labeled with Hoechst 33342 (Fig. 1C).

3.2. Establishment of spheroids with intrinsic CA IX expression

Although the induction of hypoxia by $CoCl_2$ creates a condition and a model relevant for the hypoxic tumor cores it is still not representative of the intrinsically hypoxic tumor cells in the core of the tumor. We therefore established conditions for glioblastoma spheroid formation in 3D with such cores. Representative spheroids formed from different cell number and at different times are shown in Fig. S2. These spheroids contain hypoxic cores as the *in situ* glioblastoma tumors. Spheroids seeded with smaller number of cells (5000 cells) grew at much faster rate than those formed from larger number of cells (10,000 and 20,000 cells) (Fig. S2A). Regardless of the initial number of seeded cells, the growth rate dramatically dropped once the spheroids reached a certain volume ($\sim 8 \times 10^6$ μm^3) after 7 days (Fig. S2B).

Having seen the increase in the size of spheroids over time (Fig. S2), we assessed CA IX expression and related it to the spheroid sizes and duration of their growth. Cell lysates collected from U251N spheroids of different sizes (*i.e.* different cell number from 5000 to 20,000) and grown over different time periods (4–16 days) were analyzed by Western blots. CA IX was expressed in all spheroids but the level of expression was clearly cell number and time dependent (Fig. S2C and D). The most significant CA IX expression was found in spheroids made of 50,000 cells and those that were grown for over 16 days (Fig. S2D) ($p < 0.01$).

3.3. Effect of combination of ATZ and TMZ treatment on U251N spheroids

We next, tested whether inhibition of CA IX in spheroids correlated with glioblastoma cell death. Spheroids were treated with CA IX inhibitor ATZ (100 μM) or anti-CA IX antibody (5 nM), alone or in combination with TMZ (100 μM) for 1–6 days. One-day treatments did not increase cell death relative to that of the untreated control (Fig. 2B). After 3 days of drug treatments, differences in viability were remarkable but only with ATZ or TMZ in combination (0.38 ± 0.02 a.u., $p < 0.05$), whereas drugs alone did not significantly enhance cell death. Even greater differences were measured after 6 day treatments in combination (1.28 ± 0.06 a.u., $p < 0.0001$). In contrast, the treatments with the antibody alone or in combination with TMZ did not significantly enhance cell death (Fig. 2B).

3.4. ATZ micellar nano-delivery system

ATZ is poorly soluble in water, it is photolabile [34], and it strongly binds to serum proteins [35]. Therefore, we prepared and characterized ATZ incorporated into polymeric micelles. ATZ (not incorporated into micelles) was dissolved in DMSO to prevent the drug from precipitation. Dissolved ATZ easily reached the cell plasma membrane and the interior. However, only modest cytotoxic effect was attained with ATZ concentrations up to 4 mM (Fig. S4). In contrast, ATZ incorporation into nanocarrier provided markedly higher local ATZ concentrations resulting with greater cytotoxic effect. In addition, ATZ incorporation into nanocarrier micelles reduced non-specific serum protein binding of ATZ. The major attraction of ATZ in nanocarrier was that it reached the hypoxic core more effectively than freely diffusible drug.

ATZ-loaded micelles were prepared by the co-solvent evaporation method using commercially available, biodegradable, FDA approved poly(ethylene glycol)-poly(lactic-*co*-glycolic acid) amphiphilic polymers (PEG_{2000}-$PLGA_{4000}$). Non-encapsulated ATZ was removed by centrifugation. The micelle sizes and size distributions were characterized by asymmetrical flow field-flow fractionation showing the mean hydrodynamic diameter of about 30 nm with narrow size distributions (Fig. S3).

We first established concentration dependent viability of glioblastoma cells exposed to ATZ and ATZ-loaded micelles (Fig. S4). The ATZ-loaded micelles were used for treatment of the spheroids for 1–6 days, alone and in combination with TMZ. Much to our surprise, the cell death caused by encapsulated ATZ alone (0.703 ± 0.007 a.u.) or in combination with TMZ (0.73 ± 0.02 a.u.) was highly significant even after one-day treatment ($p < 0.0001$) (Fig. 3A and B). Cell death was further enhanced after 3 days of treatment while cell death caused by ATZ micelles combined with TMZ after 6 days treatment was most effective (1.00 ± 0.08 a.u., $p < 0.0001$) (Fig. 3B).

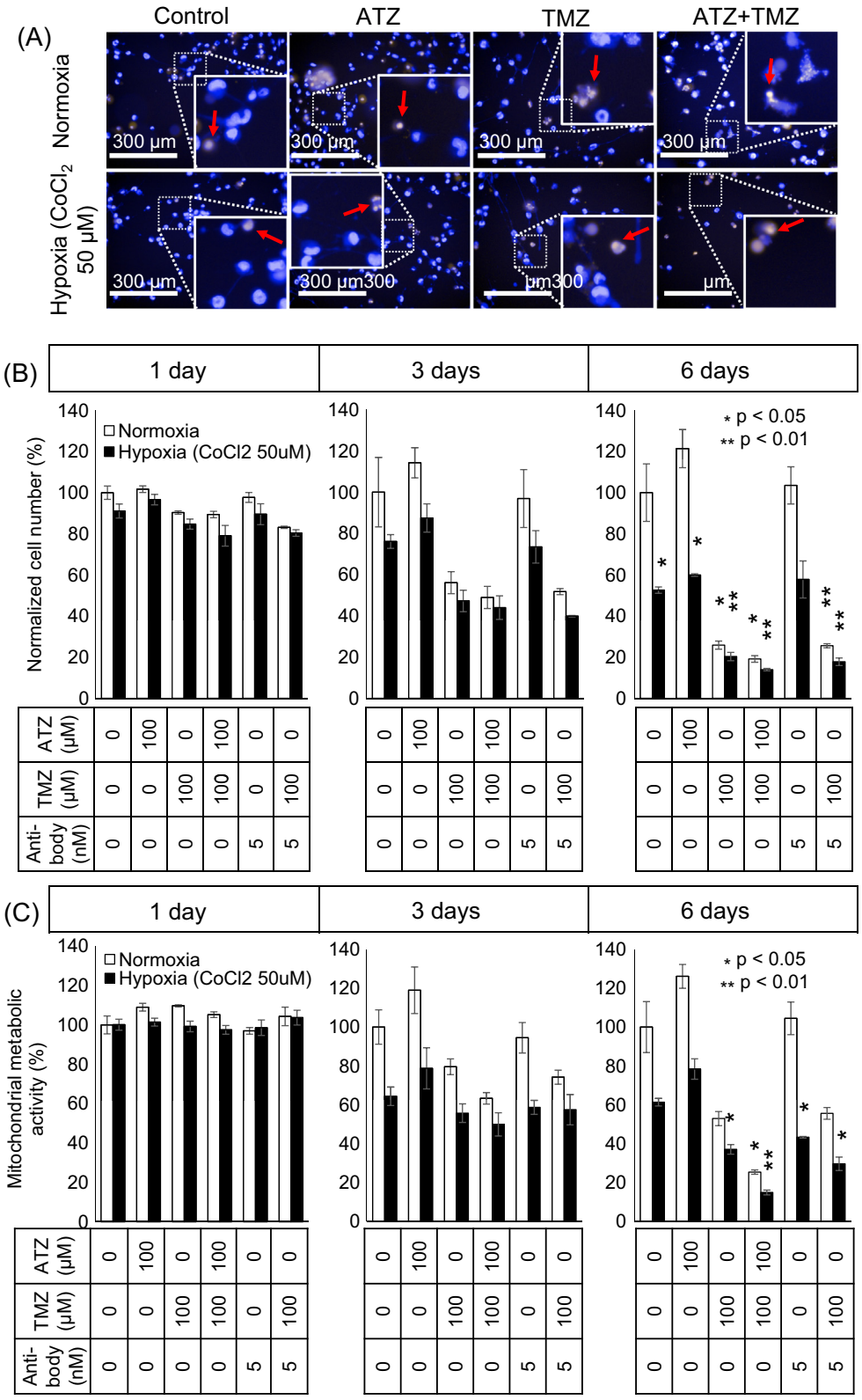

Fig. 1. CA IX inhibition combined with TMZ treatment moderately compromises viability of U251N in monolayers. (A) Photomicrograph of U251N treated cells labeled with Hoechst-33342 and PI. U251N monolayers were either exposed or not (control) to $CoCl_2$ (50 μM) for 24 h to induce hypoxia. ATZ (100 μM), anti-CA IX antibody (5 nM), TMZ (100 μM) and their combinations (concomitantly) were then added and kept for 1, 3, and 6 days. Following the treatments, Hoechst 33342 and PI were added and then cell imaging was conducted. The red arrows show the PI positive cells. (B) Quantitative data for cell viability are expressed as cell number (%) relative to the untreated cells (controls). Average values and S.E.Ms. are reported for triplicate measurements from two independent experiments. (C) Mitochondrial metabolic activity (%) of U251 cells exposed to drugs for 1–6 days. Average values and S.E.Ms. are for triplicate measurements. Statistically significant differences from control were calculated using a *t*-test and are indicated by ∗ ($p < 0.05$), ∗∗ ($p < 0.01$). (For interpretation of the references to color in this figure legend, the reader is referred to the web version of this article.)

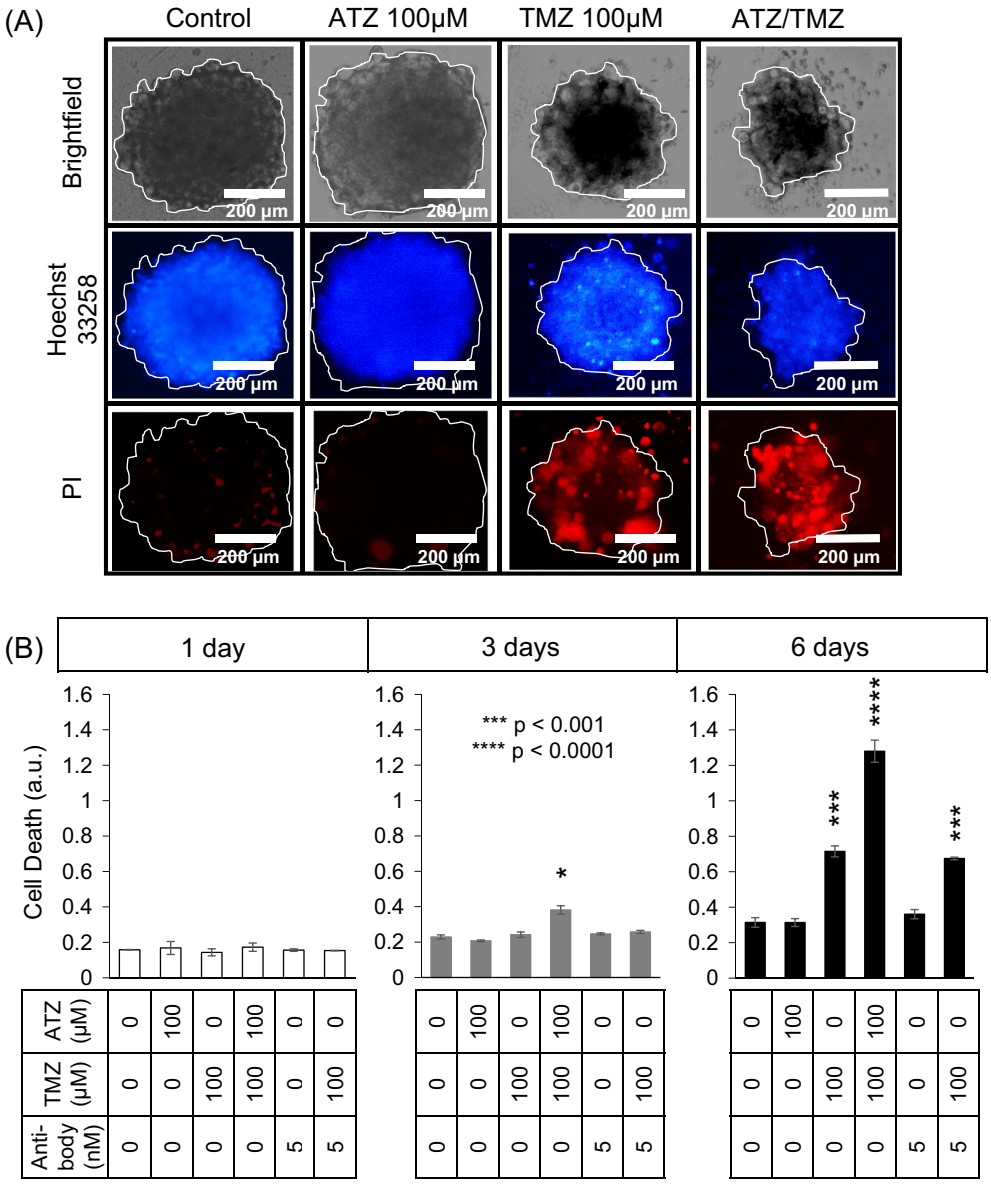

Fig. 2. Combination therapy with CA IX inhibition and temozolomide treatment promotes cell death in glioblastoma spheroids. (A) Morphological changes in U251N spheroids upon treatment with ATZ and TMZ (6 days). U251N spheroids (5 K) were developed in a 96-well plate coated with 2% agarose (Invitrogen) in serum-deprived DMEM solution. Spheroids were seeded and maintained in filtered (0.22 μm) complete DMEM medium for four days before drug treatment with ATZ (100 μM), anti-CA IX antibody (5 nM), TMZ (100 μM) and with their combination for 1, 3 and 6 days. PI and Hoechst 33342 fluorescent dyes were added 4 h prior to measurements. Following treatment, individual spheroids were imaged using a fluorescent microscope. (B) Enhancement of cell death upon combinatory treatments with ATZ and TMZ. Following treatments, PI and Hoechst 33342 fluorescent dyes were added 4 h prior to measurements. Spheroids were then carefully transferred onto a microscope slide using a pipette, and flattened under a coverslip. Imaging after flattening of the spheroids was conducted using fluorescence microscope, and fluorescence intensity was quantified using ImageJ® software [32]. The ordinate shows the relative ratio of PI to Hoechst-33342 fluorescent intensity. The abscissa shows the concentration of the drugs as indicated. Average values and S.E.M. are reported for five measurements which were repeated in at least two to five independent experiments. Statistically significant differences from control were calculated using a *t*-test and are indicated by ∗ ($p < 0.05$), ∗∗∗ ($p < 0.001$), and ∗∗∗∗ ($p < 0.0001$).

3.5. CA IX expression and effect of micelle-encapsulated ATZ in BTSCs

Inhibition of CA IX expression and activity in glioblastoma cells is not sufficient to prevent the recurrence of GBM because of the presence of BTSCs (Schematic TOC). Therefore, we investigated CA IX expression and inhibition in several types of BTSCs. They were cultured in complete Neurocult™-NS-A proliferation medium for 6–10 days. Then they were spun down and lysed. The total cell lysate was separated using denaturing conditions and transferred to the nitrocellulose membrane immunoblotted for CA IX expression. CA IX was expressed in all tested BTSCs (5.2 ± 0.2, $p < 0.01$ in 48EF and 3.3 ± 0.4, $p < 0.05$ in OPK49 cells, respectively) than in U251N spheroids (1.1 ± 0.05) after 10 days (Fig. 4).

Next, we hypothesized that the inhibition of CA IX with ATZ alone or ATZ delivered in micelles would enhance cell death in BTSCs. Although one-day treatment with ATZ alone did not significantly change the morphology of the neurospheres, when delivered by micelles, it distorted the spheroids shapes and led to detachment of the cells (Fig. 4C, indicated by red[1] arrows). More-

[1] For interpretation of color in Fig. 4, the reader is referred to the web version of this article.

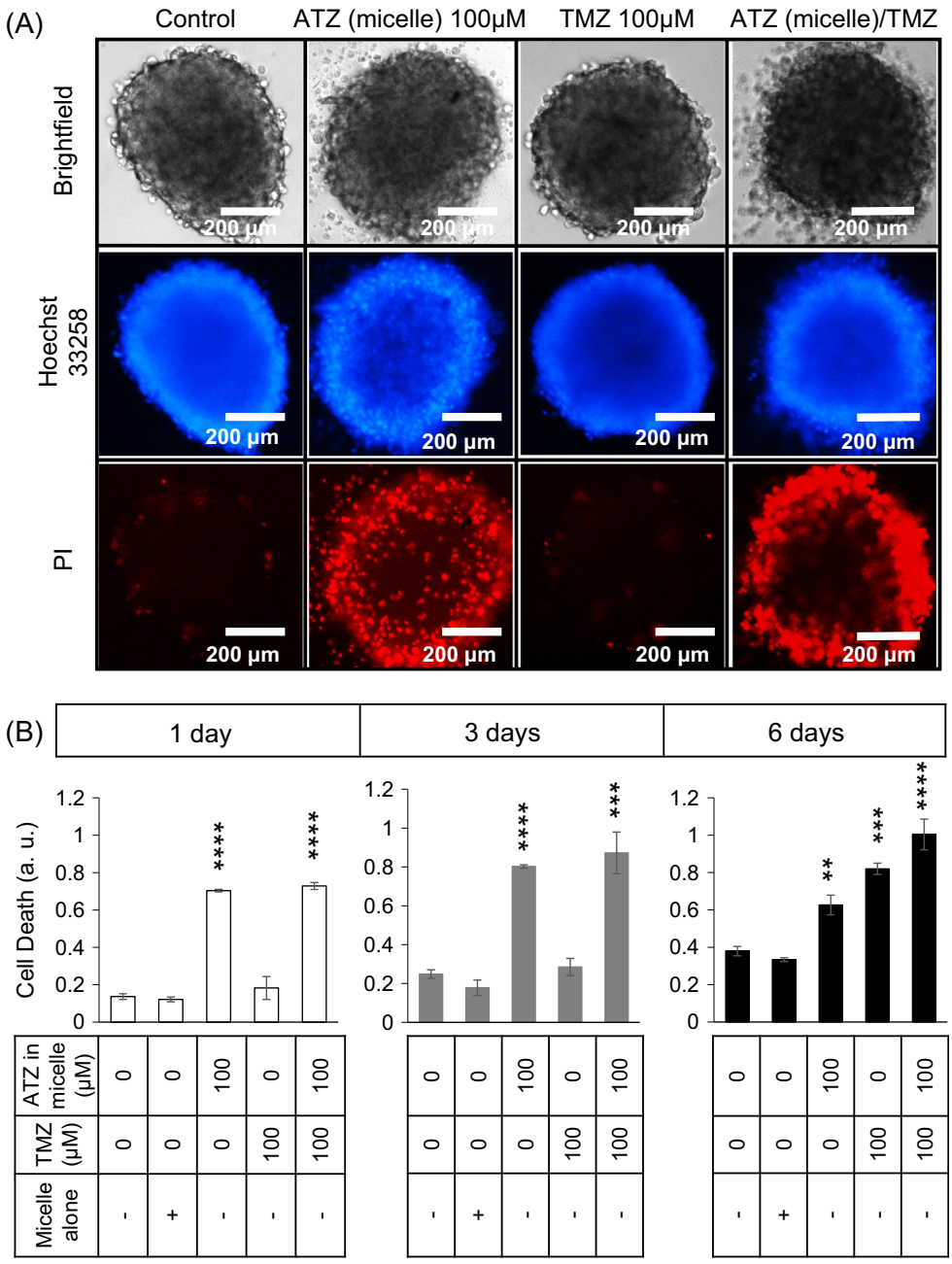

Fig. 3. Cell death caused by ATZ treatment significantly increases when delivered in micelles. (A) Morphological changes in U251N spheroids upon treatment with ATZ micelles (1 day). U251N spheroids were developed as described previously followed by drug treatments with the vehicle, ATZ micelles (100 μM), TMZ (100 μM) and with their combination for 1, 3, and 6 days. PI and Hoechst 33342 fluorescent dyes were added 4 h prior to measurements. Following treatment, individual spheroids were imaged using a fluorescent microscope. (B) Significant cell death caused by ATZ-micelles. Following treatments, PI and Hoechst 33342 fluorescent dyes were added 4 h prior to measurements. Spheroids were then carefully transferred onto a microscope slide using a pipette, and flattened under a coverslip. Imaging after flattening of the spheroids was conducted using fluorescence microscope, and fluorescence intensity was quantified using ImageJ software. The ordinate shows the relative PI to Hoechst-33342 fluorescent intensity. The abscissa shows the concentration of the drugs as indicated. Average values and S.E.Ms. are reported for five measurements which were repeated in at least two to five independent experiments. Statistically significant differences from control were calculated using a *t*-test and are indicated by ** ($p < 0.01$), *** ($p < 0.001$) and **** ($p < 0.0001$).

over, the assessment of the mitochondrial metabolic activity, using the XTT assay, indicative of no significant decrease in cell viability by ATZ alone, showed that, in contrast, when ATZ was delivered in micelles, brain tumor stem cells were completely eliminated ($p < 0.05$) (Fig. 4B).

To assess the distribution of the micelles into the tumor spheroids, we generated fluorescently labeled polymers by covalently attaching Rhodamine B to PEG-PLGA. The addition of the Rhodamine did not affect the size or size distribution after assembly of the micelles (Fig. 5A and B). U251N spheroids were exposed to fluorescent micelles for 1, 3, and 6 days. U251N spheroids internalized PEG-PLGA micelles in a dose and time-dependent manner (Fig. 5D–F).

3.6. Mechanisms of cell death through CA IX inhibition

Having seen the effect of CA IX inhibition by ATZ in combination with TMZ on the glioblastoma cell viability in both monolayers and

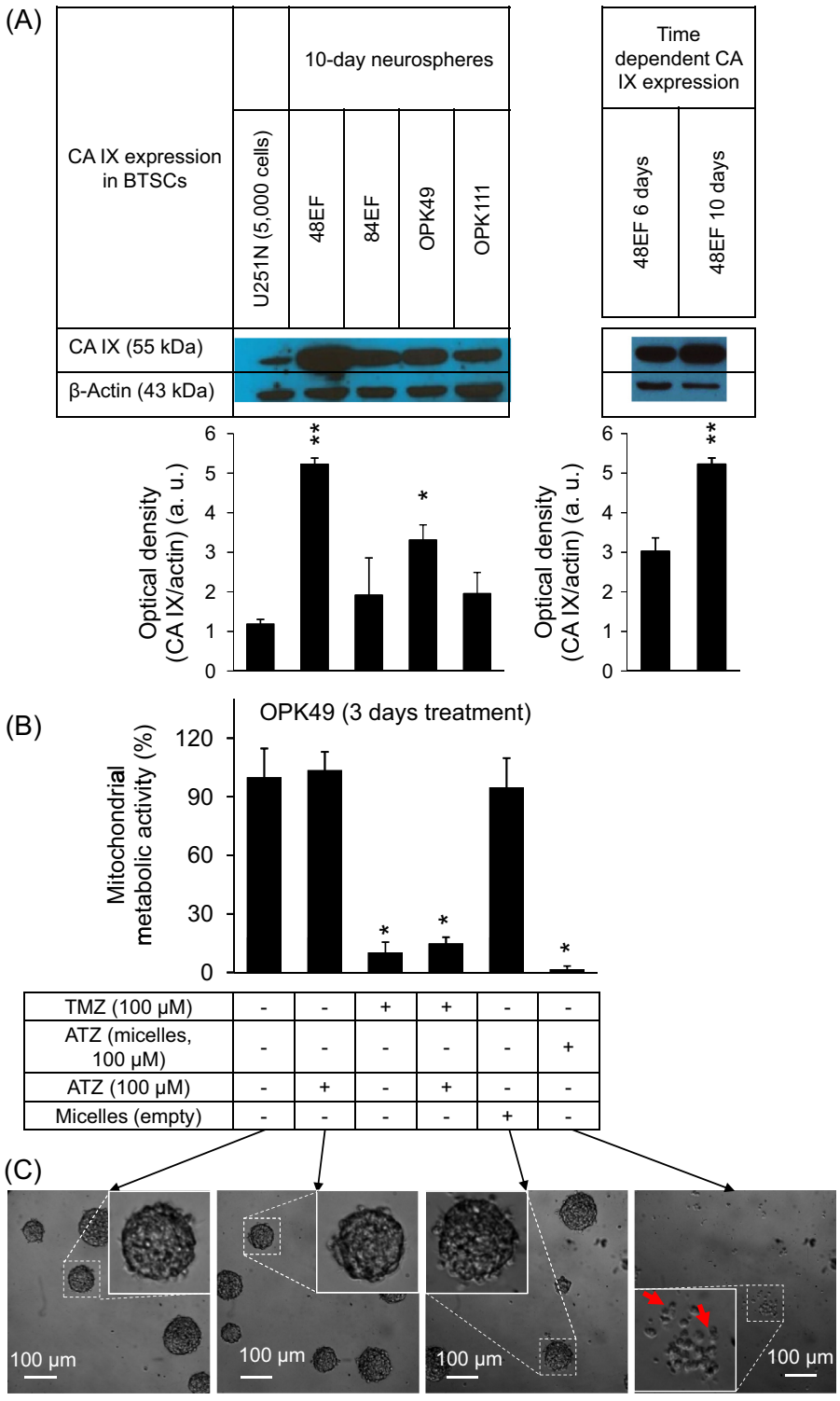

Fig. 4. CA IX is highly expressed in the BTSCs in a time dependent manner. (A) CA IX is highly expressed in BTSCs. Cells were seeded at a concentration of 200,000 cells per flask in complete Neurocult™-NS-A proliferation Medium and incubated for 6–10 days at 37 °C. Then they were collected, pelleted, washed with PBS and lysed. Total cell lysate was collected and immunoblotted for CA IX. The level of expression of CA IX is presented as the optical density of the bands over their respective actin band, the protein loading control (10 μg), on the ordinate. The abscissa shows the neurosphere's age and type as indicated. The results are representative of at least two independent experiments. Statistically significant differences from control were calculated using a *t*-test and are indicated by ∗ ($p < 0.05$) and ∗∗ ($p < 0.01$). (B) ATZ-loaded micelles compromise BTSCs viability. TMZ alone and combined with ATZ cause significant loss of mitochondrial metabolic activity. The most remarkable reduction in BTSCs viability is achieved with ATZ-loaded micelles. The changes in absorbance at 490 nm related to mitochondrial metabolic activity (ordinate) and drug treatments (abscissa) are shown for at least two independent experiments. Statistically significant differences from control were calculated using a *t*-test and are indicated by ∗ ($p < 0.05$). (C) Photomicrographs of BTSC spheres exposed to ATZ and micelle-encapsulated ATZ.

spheroids, we investigated the changes in some of cell death markers. Since the changes in glioblastoma viability were most remarkable after 6 days, the cells were collected and analyzed for the biomarker analysis. We hypothesized that caspase-3, an established marker of apoptosis, is activated by the combinatory treatments with ATZ and TMZ in both 2D and 3D models. Caspase-3

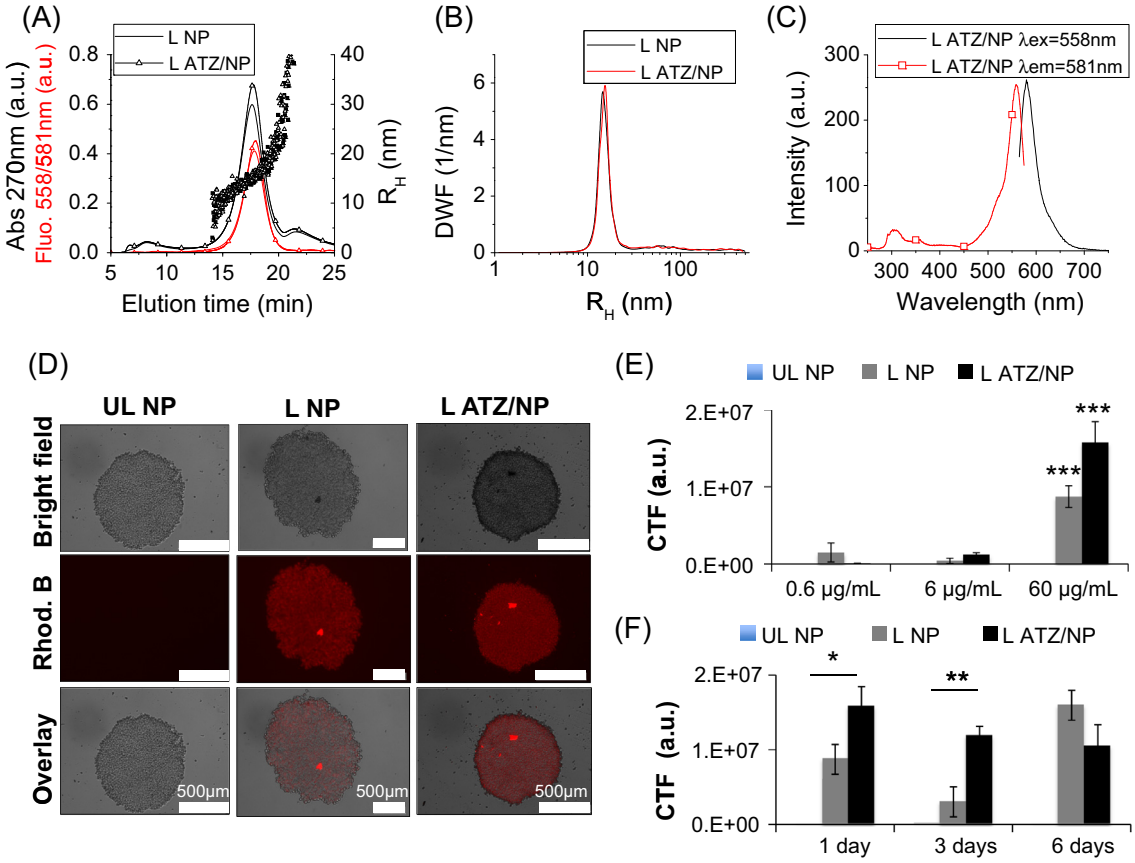

Fig. 5. Fluorescently labeled micelle internalization by spheroids. (A) Fractograms showing the absorbance (black) and fluorescence signal (red) of empty and acetazolamide-loaded rhodamine-labeled micelles (L NP and L ATZ/NP, respectively). Hydrodynamic sizes (dots) are reported on the right y-axis. (B) Size distribution calculated from the fractograms in (A) of the labeled micelles empty (black) or containing acetazolamide (red). (C) Fluorescence excitation (red and square) and emission (black) spectra of the loaded-micelles containing acetazolamide. (D) U251N spheroids (5 K) were treated with unlabeled micelles (UL NP), Rhodamine B labeled uncharged micelles (L NP) and acetazolamide (ATZ) charged Rhodamine B labeled micelles (L ATZ/NP) for 1, 3, and 6 days. Following treatment, individual spheroids were imaged using a fluorescent microscope. (E) Total spheroid fluorescence corrected for background fluorescence (ordinate, FI, a.u.) is shown for treatments with 0.6 µg/mL micelles (1 µM ATZ), 6 µg/mL micelles (10 µM ATZ), and 60 µg/mL micelles (100 µM ATZ) after 1 day. (F) Corrected total fluorescence (CTF) of spheroids incubated with 60 µg/mL unlabeled micelles (100 µM ATZ), labeled micelles, and labeled acetazolamide-containing micelles for 1 day, 3 days, and 6 days. After the treatment, spheroids were flattened and imaged using fluorescence microscope, and CTF was quantified using ImageJ software. The ordinate shows corrected total fluorescent intensity. The abscissa shows duration of the treatment. Average values and S.E.Ms. are reported for three measurements which were repeated in at least two to five independent experiments. Statistically significant differences from control were calculated using two-way ANOVA and are indicated by ** ($p < 0.01$), *** ($p < 0.001$) and **** ($p < 0.0001$). (For interpretation of the references to color in this figure legend, the reader is referred to the web version of this article.)

activity was measured using a fluorescent-based caspase-3 assay kit (refer to material and method). The principle of this assay is the cleavage of the caspase-3 substrate (Z-DEVD-R110 substrate) by activated caspase-3 (Fig. 6D).

Caspase-3 activity was increased with $CoCl_2$ treatment in 2D cultures and this effect was significantly enhanced with ATZ and TMZ cotreatment ($p < 0.0001$) (Fig. 6A). Monotherapy in spheroids was ineffective but ATZ combined with TMZ significantly increased caspase-3 activity after 6 days treatment (Fig. 6B).

To further investigate the mechanism of cell death, we measured BAX, a biomarker of apoptosis upstream of caspase-3. U251N spheroids (4 days old) were treated with ATZ, TMZ and their combination. Spheroids were then collected and lysed. The total cell lysate was immunoblotted for BAX expression. ATZ alone did not significantly change BAX expression, though TMZ did enhance BAX expression significantly (1.3 ± 0.2 $p < 0.05$). Nevertheless, the highest BAX expression was measured for cells co-treated with ATZ and TMZ (1.8 ± 0.5; $p < 0.05$) (Fig. 6C).

4. Discussion

In the present study, we evaluated the effectiveness of combination therapy in 2D and 3D (spheroid) glioblastoma models and Brain Tumor Stem Cells (BTSC). We investigated whether temozolomide anticancer effect could be augmented by the inhibition of CA IX with ATZ incorporated into polymeric micelles. Lastly, we assessed the expression and activity of several proteins implicated in the mechanisms of cell death induced by the employed therapeutics.

CA IX is a transmembrane enzyme which catalyzes the reversible conversion of carbon dioxide to carbonic acid ($CO_2 + H_2O$ to HCO_3^- and H^+). The expression of CA IX is restricted in normal cells while it is overexpressed in hypoxic tumors and particularly in glioblastoma [24]. CA IX is, a transmembrane protein involved in pH homeostasis in hypoxic tumors [8,9].

In order to study the role of CA IX and the effect of its inhibition in the context of GBM, several *ex vivo* model systems were explored: cancer cell monolayers (2D culture), cancer cell spheroids (3D culture) and brain tumor stem cell neurospheres (3D culture). *In vivo* GBM models have previously been used for the screening of candidate anticancer agents, but the molecular mechanisms remain unclear [37].

Hypoxic cores are common in 3D tumors but in 2D cultures hypoxic conditions are generated in hypoxic chambers or chemically with $CoCl_2$ [38–40]. We used $CoCl_2$ to induce hypoxia and upregulation of CA IX in GBM cell culture monolayers. Our results

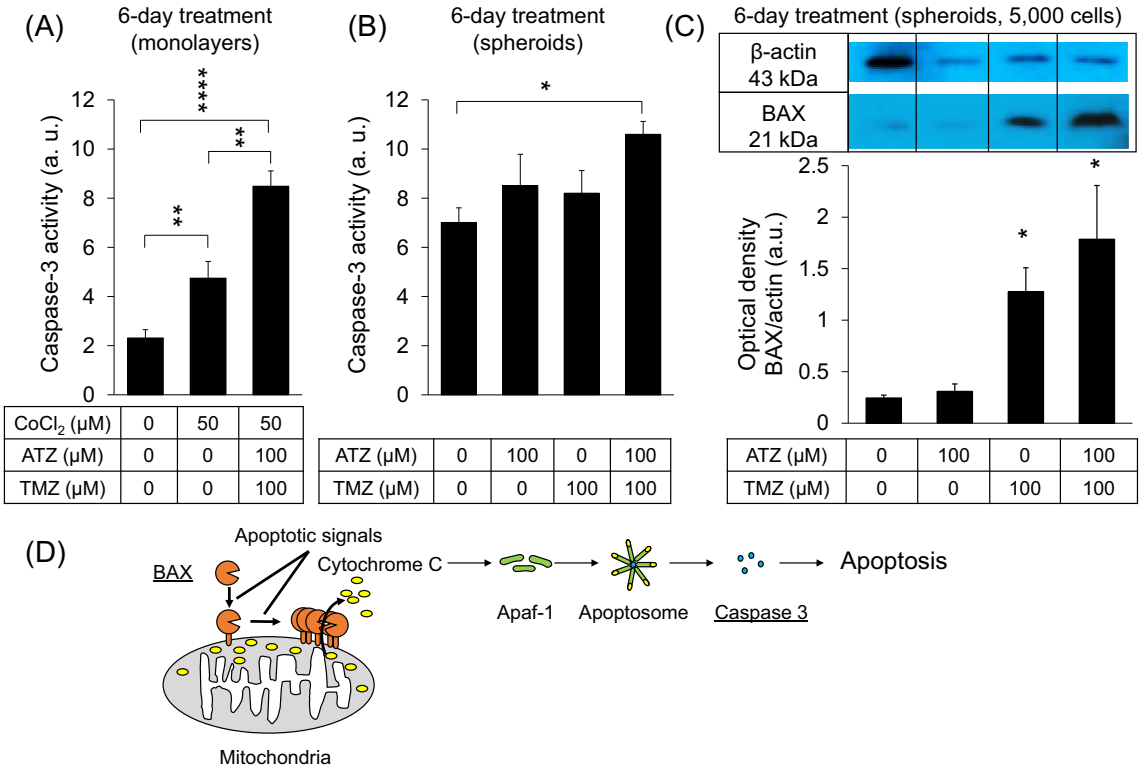

Fig. 6. (A and B) Caspase-3 activity increases in U251N glioblastoma cells upon combinatory treatment with ATZ and TMZ increases. (A) Significant increase in caspase-3 activity upon treatment for 6 days with ATZ and TMZ. U251N monolayers were grown in 6-well-plates in serum containing DMEM for 24 h. Cells were then treated with either no treatment (control) or $CoCl_2$ (50 μM) for 24 h to induce hypoxia. Then cells were exposed to the following: no treatment, ATZ (100 μM) and TMZ (100 μM) concomitant treatment for 6 days. Following the treatments, the cells were collected and were either counted or centrifuged at 12,000 rpm for 4 min. (B) U251N spheroids (5 K) were developed in a 96-well plate coated with 2% agarose in serum-deprived DMEM solution. They were seeded and maintained in filtered (0.22 μm) complete DMEM medium for four days before drug treatment with ATZ (100 μM), TMZ (100 μM), and with their combination (concomitantly) for 6 days. Following the treatments, spheroids were collected and centrifuged. EnzCheck Caspase-3 assay kit #2 was then used for both monolayers and spheroids. The fluorescence signals (excitation/emission ~496/520 nm) were measured by a spectrofluorometer (FLUOstar OPTIMA). The fluorescent signals (caspase-3 activity) were then normalized to the cell number and presented as above on the ordinate. The abscissa shows the drug concentrations. The results are representative of at least two independent experiments. Statistically significant differences from control were calculated using a *t*-test and are indicated by ∗ ($p < 0.05$), ∗∗ ($p < 0.01$) and ∗∗∗∗ ($p < 0.0001$). (C) BAX expression in GBM spheroids is enhanced upon ATZ and TMZ combinatory treatment. Significant increase in BAX expression upon treatment with ATZ and TMZ. U251 spheroids were developed as described previously. They were then treated with ATZ (100 μM), TMZ (100 μM) and with their combination for 6 days. Following the treatment spheroids were picked up by a pipette, centrifuged and lysed. Total cell lysate was collected and immunoblotted for BAX. The level of expression of BAX is presented as the optical density of the bands over their respective actin band, protein loading control (10 μg), on the ordinate. The abscissa shows the concentrations of the drugs as indicated. The results are representative of at least three independent experiments. Statistically significant differences from control were calculated using a *t*-test and are indicated by ∗ ($p < 0.05$). (D) Schematic of BAX expression and Baxosome formation leading to caspase-3 activation and apoptotic cell death. Adapted from Dewson and Kluck [36].

concur with results in previous studies with GBM cell lines including U251N [10,39,41].

It is now widely established that tumor cell behavior and signaling cascades are substantially different in 2D and 3D cultures [42,43]. 3D cultures mimic more closely the *in vivo* environment in many critical ways than 2D cultures [43]. One of the important characteristics of the 3D models (spheroids) is the formation of a hypoxic core within the spheroids. Our results clearly showed a significant CA IX expression as a result of hypoxia. CA IX expression significantly increased in a time and size dependent manner (Fig. S2C and D). Our results, are consistent with those of Imamura et al. hypoxic 3D multicellular breast cancer spheroids (three cell lines: BT-549, BT-474 and T-47D) [44]. In our studies, spheroids exposed to the monotherapy (inhibitors of CA IX: ATZ, and CA IX antibodies) did not significantly enhance cell death. Similar findings were obtained by Das et al., in T98G and U87MG glioblastoma cell lines [45]. In contrast, cell death was significantly enhanced in the spheroids co-treated with ATZ and TMZ. It is conceivable that an increase in the extracellular pH and reduction of intracellular pH by ATZ promoted TMZ activation in the extracellular microenvironment, its cell entry [46], and consequently an enhanced TMZ tumor cell death [47].

Models of heterogeneous tumor cell populations are needed for testing anticancer therapies [48–50]. Human BTSC are a slowly-dividing, small population within a heterogeneous glioblastoma which can recapitulate a whole tumor and differentiate into other specific GBM subpopulations [51]. Human BTSC tend to preferentially reside within the hypoxic core of tumor mass [52]. Considering their preferential location, we anticipated high CA IX expression. Our results show significantly higher CAIX expression in 48EF and OPK49 BTSCs ($p < 0.01$ and $p < 0.05$, respectively) in comparison with GBM U251N cells. The enhancement of CA IX expression in BTSC was time dependent. Consistent with our findings are those in 3D esophageal squamous carcinoma stem cell lines TE2 and TTn where CA IX in the 7-day old spheroids was significantly increased [53]. The very high and specific expression of CA IX in the BTSC is an interesting finding indicating usefulness of BTSC in drug development for reoccurring GBM.

One of the limitations in treating GBM is poor drug accessibility to the tumor. To enhance local therapeutic concentration different nano-delivery systems were developed and some of them are in clinical trials [54,55]. Polymeric micelles showed an improved drug efficacy in glioblastoma mice models [56,57]. Considering limited photostability, low solubility in aqueous medium, and high protein

binding of ATZ, we incorporated ATZ into micelles and tested them in the 3D models (spheroids and neurospheres). As opposed to the free ATZ, which did not affect cell viability after one day, the ATZ micelles caused a significant increase in cell death even after one-day treatment in U251N spheroids. Similar to U251N spheroids, the OPK49 BTSC viability was not significantly reduced by free ATZ, whereas ATZ micelles completely eradicated the cells after 3 days of treatment. The enhanced effectiveness of ATZ micelles is likely because of ATZ protection and slow release in tumor. Secondly, as opposed to free ATZ which can diffuse in and out of the cells [58], ATZ micelles are retained for a longer time period. Thirdly, unincorporated ATZ precipitates in aqueous medium (whereas micelle-incorporated ATZ does not). Fluorescent micelles containing ATZ showed that the micelles were taken up by cells in spheroids and reduced viability of U251N and BTSCs.

Modes of cell death induced by ATZ and TMZ include at least apoptosis, necrosis and necroptosis. We detected picnotic nuclei and significantly enhanced caspase-3 activity, indicative of apoptotic cell death. We have previously shown that in transfected glioblastoma cells, curcumin but not TMZ, causes a significant activation of caspase-3 [59]. In the present study, it is worth noting that the increase in caspase-3 activity with the combined treatment in comparison with the untreated controls was markedly higher in the 2D monolayers relative to the 3D spheroids, apparently more resistant to the anticancer treatment [44].

Although caspase-3 is an established biomarker of apoptosis and necessary for the acquisition of the apoptotic morphology, it is not sufficient to define apoptosis [60–62]. Thus as a follow-up experiment, we examined the level of BAX expression after treatment of U251N spheroids with ATZ and TMZ for 6 days. BAX is a pro-apoptotic member of Bcl-2 family. BAX is translocated from the cytosol to the mitochondrial outer membrane (OM) forming pores leading to the release of pro-apoptotic factors such as cytochrome *c* and subsequent cell death [36]. Recent studies clearly show Bax clustering and pore formation by super-resolution microscopy [63].

BAX overexpression and enhanced caspase-3 activity suggest that apoptosis is one of the mechanisms of cell death caused by ATZ and TMZ treatment in the glioblastoma cell models. Consistent with our results, Das et al., showed apoptosis in T98G and U87MG glioblastoma cells with ATZ or TMZ separate treatments [45].

In addition to apoptotic cell death, labeling with propidium iodide of GBM and BTSC indicated significant fluorescent signals indicative of disrupted plasma membrane. An intense fluorescence was found both in cells with picnotic and fragmented nuclei indicating two additional modes of cell death, *i.e.* necroptosis and necrosis.

Necroptosis is characterized with permeable plasma membrane and detectable biomarkers of apoptosis including caspase 3 and picnotic nuclei [60]. Leaky membranes, swollen soma and fragmented nuclei are often found in necrotic cells. Imaging of fluorescent nuclear and membrane labels combined with biochemical biomarkers suggest multiple modes of cell death of GBM and stem cells treated with TMZ and ATZ. Another possibility is that glioma and brain tumor stem cells were partly dying by methuosis when exposed to micelle-incorporated drugs. Methuosis is a consequence of excessive pinocytosis and it would be worth testing in brain tumor stem cells by combining CA IX inhibitors and vacquinol-1. The key features of this mode of cell death are reviewed (Non-apoptotic cell death associated with perturbations of macropinocytosis [64]).

Overall, the results from this research show that combination therapy is superior to monotherapy for elimination of not only glioblastoma cells but also human brain tumor stem cells. Combined therapeutics activate several modes of cell death which is markedly enhanced by incorporation in nano-carriers. Further studies are warranted to delineate molecular mechanisms implicated in the multimodal cell death of glioma and brain tumor stem cells in experimental animals.

Author contributions

PL performed the viability experiments on BTSC. AM prepared the various micelles and performed their physico-chemical characterization. AA performed all the other experiments on the monolayers and spheroids including the Western blots and viability experiment. GM performed micelle internalization studies in U251N spheroids. DM and JWG conceived the experiments, discussed them with students and completed the final draft of the manuscript. All authors read and approved the final version of the manuscript prior to the submission.

Acknowledgments

The authors acknowledge the financial support to Canadian Institutes for Health Research (CIHR), Canada. AA is the recipient of MITACS Accelerate (also an internship from KalGene Pharmaceuticals), Natural Sciences and Engineering Research Council of Canada (NSERC CGS M) and Graduate Excellence Fellowship (GEF).

Appendix A. Supplementary material

Supplementary data associated with this article can be found, in the online version, at http://dx.doi.org/10.1016/j.ejpb.2016.09.018.

References

[1] CBTRUS, Statistical report: primary brain tumors in the United States, 2000–2004, Central Brain Tumor Registry of the United States: Chicago, 2008.
[2] S.K. Carlsson, S.P. Brothers, C. Wahlestedt, Emerging treatment strategies for glioblastoma multiforme, EMBO Mol. Med. 6 (11) (2014) 1359–1370.
[3] K.M. Bailey, J.W. Wojtkowiak, A.I. Hashim, R.J. Gillies, Targeting the metabolic microenvironment of tumors, Adv. Pharmacol. 65 (2012) 63–107.
[4] U. Lendahl, K.L. Lee, H. Yang, L. Poellinger, Generating specificity and diversity in the transcriptional response to hypoxia, Nat. Rev. Genet. 10 (12) (2009) 821–832.
[5] M.C. Brahimi-Horn, G. Bellot, J. Pouyssegur, Hypoxia and energetic tumour metabolism, Curr. Opin. Genet. Dev. 21 (1) (2011) 67–72.
[6] R.J. Gillies, I. Robey, R.A. Gatenby, Causes and consequences of increased glucose metabolism of cancers, J. Nucl. Med. 49 (Suppl 2) (2008) 24s–42s.
[7] P. DelNero, M. Lane, S.S. Verbridge, B. Kwee, P. Kermani, B. Hempstead, A. Stroock, C. Fischbach, 3D culture broadly regulates tumor cell hypoxia response and angiogenesis via pro-inflammatory pathways, Biomaterials 55 (2015) 110–118.
[8] S. Kaluz, M. Kaluzova, S.Y. Liao, M. Lerman, E.J. Stanbridge, Transcriptional control of the tumor- and hypoxia-marker carbonic anhydrase 9: a one transcription factor (HIF-1) show?, Biochim Biophys. Acta 1795 (2) (2009) 162–172.
[9] P.C. McDonald, J.Y. Winum, C.T. Supuran, S. Dedhar, Recent developments in targeting carbonic anhydrase IX for cancer therapeutics, Oncotarget 3 (1) (2012) 84–97.
[10] H.M. Said, A. Staab, C. Hagemann, G.H. Vince, A. Katzer, M. Flentje, D. Vordermark, Distinct patterns of hypoxic expression of carbonic anhydrase IX (CA IX) in human malignant glioma cell lines, J. Neurooncol. 81 (1) (2007) 27–38.
[11] J. Zavada, Z. Zavadova, J. Pastorek, Z. Biesova, J. Jezek, J. Velek, Human tumour-associated cell adhesion protein MN/CA IX: identification of M75 epitope and of the region mediating cell adhesion, Br. J. Cancer 82 (11) (2000) 1808–1813.
[12] R. Opavsky, S. Pastorekova, V. Zelnik, A. Gibadulinova, E.J. Stanbridge, J. Zavada, R. Kettmann, J. Pastorek, Human MN/CA9 gene, a novel member of the carbonic anhydrase family: structure and exon to protein domain relationships, Genomics 33 (3) (1996) 480–487.
[13] P. Swietach, R.D. Vaughan-Jones, A.L. Harris, Regulation of tumor pH and the role of carbonic anhydrase 9, Cancer Metastasis Rev. 26 (2) (2007) 299–310.
[14] T. Wingo, C. Tu, P.J. Laipis, D.N. Silverman, The catalytic properties of human carbonic anhydrase IX, Biochem. Biophys. Res. Commun. 288 (3) (2001) 666–669.
[15] F.E. Lock, P.C. McDonald, Y. Lou, I. Serrano, S.C. Chafe, C. Ostlund, S. Aparicio, J. Y. Winum, C.T. Supuran, S. Dedhar, Targeting carbonic anhydrase IX depletes breast cancer stem cells within the hypoxic niche, Oncogene 32 (44) (2013) 5210–5219.

[16] T. Fiaschi, E. Giannoni, M.L. Taddei, P. Cirri, A. Marini, G. Pintus, C. Nativi, B. Richichi, A. Scozzafava, F. Carta, E. Torre, C.T. Supuran, P. Chiarugi, Carbonic anhydrase IX from cancer-associated fibroblasts drives epithelial-mesenchymal transition in prostate carcinoma cells, Cell Cycle 12 (11) (2013) 1791–1801.
[17] D.A. Cavazos, A.J. Brenner, Hypoxia in astrocytic tumors and implications for therapy, Neurobiol. Dis. 85 (2016) 227–233.
[18] L. Dubois, S. Peeters, N.G. Lieuwes, N. Geusens, A. Thiry, S. Wigfield, F. Carta, A. McIntyre, A. Scozzafava, J.M. Dogne, C.T. Supuran, A.L. Harris, B. Masereel, P. Lambin, Specific inhibition of carbonic anhydrase IX activity enhances the in vivo therapeutic effect of tumor irradiation, Radiother. Oncol. 99 (3) (2011) 424–431.
[19] S. Ivanov, S.Y. Liao, A. Ivanova, A. Danilkovitch-Miagkova, N. Tarasova, G. Weirich, M.J. Merrill, M.A. Proescholdt, E.H. Oldfield, J. Lee, J. Zavada, A. Waheed, W. Sly, M.I. Lerman, E.J. Stanbridge, Expression of hypoxia-inducible cell-surface transmembrane carbonic anhydrases in human cancer, Am. J. Pathol. 158 (3) (2001) 905–919.
[20] C. Potter, A.L. Harris, Hypoxia inducible carbonic anhydrase IX, marker of tumour hypoxia, survival pathway and therapy target, Cell Cycle 3 (2) (2004) 164–167.
[21] N. Robertson, C. Potter, A.L. Harris, Role of carbonic anhydrase IX in human tumor cell growth, survival, and invasion, Cancer Res. 64 (17) (2004) 6160–6165.
[22] S.K. Parks, J. Chiche, J. Pouyssegur, PH control mechanisms of tumor survival and growth, J. Cell. Physiol. 226 (2) (2011) 299–308.
[23] M. Kanamala, W.R. Wilson, M. Yang, B.D. Palmer, Z. Wu, Mechanisms and biomaterials in pH-responsive tumour targeted drug delivery: a review, Biomaterials 85 (2016) 152–167.
[24] M.A. Proescholdt, M.J. Merrill, E.M. Stoerr, A. Lohmeier, F. Pohl, A. Brawanski, Function of carbonic anhydrase IX in glioblastoma multiforme, Neuro Oncol. 14 (11) (2012) 1357–1366.
[25] F. Cianchi, M.C. Vinci, C.T. Supuran, B. Peruzzi, P. De Giuli, G. Fasolis, G. Perigli, S. Pastorekova, L. Papucci, A. Pini, E. Masini, L. Puccetti, Selective inhibition of carbonic anhydrase IX decreases cell proliferation and induces ceramide-mediated apoptosis in human cancer cells, J. Pharmacol. Exp. Ther. 334 (3) (2010) 710–719.
[26] L. Dubois, K. Douma, C.T. Supuran, R.K. Chiu, M.A. van Zandvoort, S. Pastorekova, A. Scozzafava, B.G. Wouters, P. Lambin, Imaging the hypoxia surrogate marker CA IX requires expression and catalytic activity for binding fluorescent sulfonamide inhibitors, Radiother. Oncol. 83 (3) (2007) 367–373.
[27] Y. Li, H. Wang, E. Oosterwijk, C. Tu, K.T. Shiverick, D.N. Silverman, S.C. Frost, Expression and activity of carbonic anhydrase IX is associated with metabolic dysfunction in MDA-MB-231 breast cancer cells, Cancer Invest. 27 (6) (2009) 613–623.
[28] Y. Lou, P.C. McDonald, A. Oloumi, S. Chia, C. Ostlund, A. Ahmadi, A. Kyle, U. Auf dem Keller, S. Leung, D. Huntsman, B. Clarke, B.W. Sutherland, D. Waterhouse, M. Bally, C. Roskelley, C.M. Overall, A. Minchinton, F. Pacchiano, F. Carta, A. Scozzafava, N. Touisni, J.Y. Winum, C.T. Supuran, S. Dedhar, Targeting tumor hypoxia: suppression of breast tumor growth and metastasis by novel carbonic anhydrase IX inhibitors, Cancer Res. 71 (9) (2011) 3364–3376.
[29] M. Roger, A. Clavreul, M.C. Venier-Julienne, C. Passirani, C. Montero-Menei, P. Menei, The potential of combinations of drug-loaded nanoparticle systems and adult stem cells for glioma therapy, Biomaterials 32 (8) (2011) 2106–2116.
[30] J.J. Kelly, O. Stechishin, A. Chojnacki, X. Lun, B. Sun, D.L. Senger, P. Forsyth, R.N. Auer, J.F. Dunn, J.G. Cairncross, I.F. Parney, S. Weiss, Proliferation of human glioblastoma stem cells occurs independently of exogenous mitogens, Stem Cells 27 (8) (2009) 1722–1733.
[31] R.S. Dhanikula, A. Argaw, J.F. Bouchard, P. Hildgen, Methotrexate loaded polyether-copolyester dendrimers for the treatment of gliomas: enhanced efficacy and intratumoral transport capability, Mol. Pharm. 5 (1) (2008) 105–116.
[32] C.A. Schneider, W.S. Rasband, K.W. Eliceiri, NIH Image to ImageJ: 25 years of image analysis, Nat. Meth. 9 (7) (2012) 671–675.
[33] J.M. Bernstein, T.D. Andrews, N.J. Slevin, C.M. West, J.J. Homer, Prognostic value of hypoxia-associated markers in advanced larynx and hypopharynx squamous cell carcinoma, Laryngoscope 125 (1) (2015) E8–E15.
[34] F. Vargas, M.V. Hisbeth, J.K. Rojas, Photolysis and photosensitized degradation of the diuretic drug acetazolamide, J. Photochem. Photobiol., A 118 (1) (1998) 19–23.
[35] I.H. Gomolin, D.J. Chapron, Elucidating the relationship between acetazolamide plasma protein binding and renal clearance using an albumin infusion, J. Clin. Pharmacol. 32 (11) (1992) 1028–1032.
[36] G. Dewson, R.M. Kluck, Mechanisms by which Bak and Bax permeabilise mitochondria during apoptosis, J. Cell Sci. 122 (Pt 16) (2009) 2801–2808.
[37] S.S. Rao, J.J. Lannutti, M.S. Viapiano, A. Sarkar, J.O. Winter, Toward 3D biomimetic models to understand the behavior of glioblastoma multiforme cells, Tissue Eng. Part B Rev. 20 (4) (2014) 314–327.
[38] T. Matsubara, G.R. Diresta, S. Kakunaga, D. Li, J.H. Healey, Additive influence of extracellular pH, oxygen tension, and pressure on invasiveness and survival of human osteosarcoma cells, Front. Oncol. 3 (2013) 199.
[39] S. Teppo, E. Sundquist, M. Vered, H. Holappa, J. Parkkisenniemi, T. Rinaldi, P. Lehenkari, R. Grenman, D. Dayan, J. Risteli, T. Salo, P. Nyberg, The hypoxic tumor microenvironment regulates invasion of aggressive oral carcinoma cells, Exp. Cell Res. 319 (4) (2013) 376–389.
[40] J. Chen, C. Rocken, J. Hoffmann, S. Kruger, U. Lendeckel, A. Rocco, S. Pastorekova, P. Malfertheiner, M.P. Ebert, Expression of carbonic anhydrase 9 at the invasion front of gastric cancers, Gut 54 (7) (2005) 920–927.
[41] H.M. Said, C. Hagemann, F. Carta, A. Katzer, B. Polat, A. Staab, A. Scozzafava, J. Anacker, G.H. Vince, M. Flentje, C.T. Supuran, Hypoxia induced CA9 inhibitory targeting by two different sulfonamide derivatives including acetazolamide in human glioblastoma, Bioorg. Med. Chem. 21 (13) (2013) 3949–3957.
[42] E. Cukierman, R. Pankov, D.R. Stevens, K.M. Yamada, Taking cell-matrix adhesions to the third dimension, Science 294 (5547) (2001) 1708–1712.
[43] K.M. Yamada, E. Cukierman, Modeling tissue morphogenesis and cancer in 3D, Cell 130 (4) (2007) 601–610.
[44] Y. Imamura, T. Mukohara, Y. Shimono, Y. Funakoshi, N. Chayahara, M. Toyoda, N. Kiyota, S. Takao, S. Kono, T. Nakatsura, H. Minami, Comparison of 2D- and 3D-culture models as drug-testing platforms in breast cancer, Oncol. Rep. 33 (4) (2015) 1837–1843.
[45] A. Das, N.L. Banik, S.K. Ray, Modulatory effects of acetazolamide and dexamethasone on temozolomide-mediated apoptosis in human glioblastoma T98G and U87MG cells, Cancer Invest. 26 (4) (2008) 352–358.
[46] H.S. Friedman, T. Kerby, H. Calvert, Temozolomide and treatment of malignant glioma, Clin. Cancer Res. 6 (7) (2000) 2585–2597.
[47] P. Swietach, A. Hulikova, R.D. Vaughan-Jones, A.L. Harris, New insights into the physiological role of carbonic anhydrase IX in tumour pH regulation, Oncogene 29 (50) (2010) 6509–6521.
[48] R.C. Rennert, A.S. Achrol, M. Januszyk, S.A. Kahn, T.T. Liu, Y. Liu, D. Sahoo, M. Rodrigues, Z.N. Maan, V.W. Wong, S.H. Cheshier, S.D. Chang, G.K. Steinberg, G. R. Harsh, G.C. Gurtner, Multiple subsets of brain tumor initiating cells co-exist in glioblastoma, Stem Cells 34 (6) (2016) 1702–1707.
[49] E. Codrici, A.M. Enciu, I.D. Popescu, S. Mihai, C. Tanase, Glioma stem cells and their microenvironments: providers of challenging therapeutic targets, Stem Cells Int. 2016 (2016) 5728438.
[50] R. Sakuma, M. Kawahara, A. Nakano-Doi, A. Takahashi, Y. Tanaka, A. Narita, S. Kuwahara-Otani, T. Hayakawa, H. Yagi, T. Matsuyama, T. Nakagomi, Brain pericytes serve as microglia-generating multipotent vascular stem cells following ischemic stroke, J. Neuroinflamm. 13 (1) (2016) 57.
[51] B. Auffinger, D. Spencer, P. Pytel, A.U. Ahmed, M.S. Lesniak, The role of glioma stem cells in chemotherapy resistance and glioblastoma multiforme recurrence, Expert Rev. Neurother. 15 (7) (2015) 741–752.
[52] L. Persano, E. Rampazzo, A. Della Puppa, F. Pistollato, G. Basso, The three-layer concentric model of glioblastoma: cancer stem cells, microenvironmental regulation, and therapeutic implications, Sci. World J. 11 (2011) 1829–1841.
[53] D. Fujiwara, K. Kato, S. Nohara, Y. Iwanuma, Y. Kajiyama, The usefulness of three-dimensional cell culture in induction of cancer stem cells from esophageal squamous cell carcinoma cell lines, Biochem. Biophys. Res. Commun. 434 (4) (2013) 773–778.
[54] W. Zhu, L. Zhou, J.Q. Qian, T.Z. Qiu, Y.Q. Shu, P. Liu, Temozolomide for treatment of brain metastases: a review of 21 clinical trials, World J. Clin. Oncol. 5 (1) (2014) 19–27.
[55] J. Ruzevick, C. Jackson, J. Phallen, M. Lim, Clinical trials with immunotherapy for high-grade glioma, Neurosurg. Clin. N Am. 23 (3) (2012) 459–470.
[56] J. Kuroda, J. Kuratsu, M. Yasunaga, Y. Koga, Y. Saito, Y. Matsumura, Potent antitumor effect of SN-38-incorporating polymeric micelle, NK012, against malignant glioma, Int. J. Cancer 124 (11) (2009) 2505–2511.
[57] A.J. Li, Y.H. Zheng, G.D. Liu, W.S. Liu, P.C. Cao, Z.F. Bu, Efficient delivery of docetaxel for the treatment of brain tumors by cyclic RGD-tagged polymeric micelles, Mol. Med. Rep. 11 (4) (2015) 3078–3086.
[58] K.R. Sweeney, D.J. Chapron, P.A. Kramer, Effect of salicylate on serum protein binding and red blood cell uptake of acetazolamide in vitro, J. Pharm. Sci. 77 (9) (1988) 751–756.
[59] I. Zhang, Y. Cui, A. Amiri, Y. Ding, R.E. Campbell, D. Maysinger, Pharmacological inhibition of lipid droplet formation enhances the effectiveness of curcumin in glioblastoma, Eur. J. Pharm. Biopharm. 100 (2016) 66–76.
[60] G. Kroemer, S.J. Martin, Caspase-independent cell death, Nat. Med. 11 (7) (2005) 725–730.
[61] S. Kumar, Caspase function in programmed cell death, Cell Death Differ. 14 (1) (2007) 32–43.
[62] M. Lamkanfi, N. Festjens, W. Declercq, T. Vanden Berghe, P. Vandenabeele, Caspases in cell survival, proliferation and differentiation, Cell Death Differ. 14 (1) (2007) 44–55.
[63] L. Grosse, C.A. Wurm, C. Bruser, D. Neumann, D.C. Jans, S. Jakobs, Bax assembles into large ring-like structures remodeling the mitochondrial outer membrane in apoptosis, EMBO J. 35 (4) (2016) 402–413.
[64] W.A. Maltese, J.H. Overmeyer, Non-apoptotic cell death associated with perturbations of macropinocytosis, Front. Physiol. 6 (2015) 38.